A "Lorentz" Steerer for Ion Injection into a Penning Trap

R. Ringle [a,b,*] G. Bollen [a,b] A. Prinke [a,b] J. Savory [a,b]

P. Schury [a,b] S. Schwarz [a] T. Sun

[a] *National Superconducting Cyclotron Laboratory, East Lansing, MI, USA*

[b] *Department of Physics and Astronomy, Michigan State University, East Lansing, MI, USA*

Abstract

A technique for precise control of ion injection into a Penning trap is presented, based on the employment of an $\vec{E} \times \vec{B}$ drift motion of the ion in the strong magnetic field in which the Penning trap is located. An electric dipole field with variable strength and orientation allows for precise placement of the ion in the radial plane of the trap. This method allows for fast preparation of an ion's magnetron motion, as used, for example, in the time-of-flight cyclotron resonance detection technique.

Key words:

PACS: 21.10.Dr, 34.50.Bw, 41.85.Ja, 29.25.Rm

* Corresponding author.
Email address: ringle@nscl.msu.edu (R. Ringle).

1 Introduction

In precision Penning trap mass measurements with ions provided from external sources the transfer of the ions into the trap and the preparation of their initial motion are critical parameters. This is particularly true for mass measurements of rare isotopes, an area where Penning trap mass spectrometry has gained significant importance. The isotopes are often short-lived and only produced in minute quantities. A very-high transfer efficiency and a fast, precise preparation of the initial ion motion therefore is mandatory. During the injection of the ions into the solenoidal field of the Penning trap care has to be taken to minimize the pickup of radial (transverse) energy [1]. A well-defined initial state of the trapped-ion motion is required for the subsequent excitation with radiofrequency fields, e.g., for the determination of the ion's cyclotron frequency from which the ion's mass can be determined.

In a number of Penning trap mass spectrometers for rare isotopes (ISOLTRAP [1], CPT [2], JYFLTRAP [3], SHIPTRAP [4], and LEBIT [5]), and also in the SMILETRAP [6] experiment for highly-charged ions, a cyclotron resonance detection technique is used in which the ion motion is excited at the ion's true cyclotron frequency $\omega_c = q/m \cdot B = \omega_+ + \omega_-$, using an azimuthal, radiofrequency quadrupolar field [7,8]. Here q/m is the charge-to-mass ratio of the ion, B is the magnetic field of the Penning trap and ω_+ and ω_- are the reduced cyclotron frequency and the magnetron frequency of the ion. Prior to the excitation the ions need to be prepared such that they initially perform a magnetron motion. In resonance, i.e. $\omega_{rf} = \omega_c$, the excitation leads to a periodic beating between magnetron and cyclotron motion, similar to Rabi beating in a two-level atomic system. The application of an RF π-pulse, with

the appropriate product of excitation amplitude U_{rf} and excitation time T_{rf}, will fully convert the initial magnetron motion into cyclotron motion. This resonant effect is detected with a time-of-flight technique [9] and used for the determination of ω_c.

In all these spectrometers, the ions are delivered in a short pulse and captured in the center of the trap. Classicaly, a dipolar RF field of frequency ω_- is used to drive the ions until they perform a magnetron motion with the desired radius [7]. This dipolar excitation requires some finite amount of time, typically on the order of 10 ms. Because of imperfections in the transport of the ions into the magnetic field due to misalignments, lack of diagnostics, etc., the ion beam may not be symmetric with respect to the magnetic field axis. The subsequent capture of this off-axis beam in a Penning trap results in initial magnetron (-) and cyclotron (+) motions with amplitudes $\rho_{\pm,o}$ and phases $\phi_{\pm,o}$. The result of the subsequent quadrupolar excitation depends on these initial parameters. In order to ensure that the RF dipolar excitation always leads to a magnetron motion with the same radius the RF phase needs to be locked to the time of capture of the ion pulse[10].

For the precision Penning trap mass spectrometer of the recently commissioned LEBIT facility [5] at the NSCL a new technique has been developed to prepare the ions into their initial magnetron motion, which is very fast and simpler than the dipole excitation scheme previously employed. Named the Lorentz Steerer, the system provides precise control over the transversal position at which the ions are captured. The basic principle is illustrated in Fig. 1. A four-fold segmented cylinder is placed into the injection path of the ions on their way into the Penning trap. With voltages applied such that an electric dipole field $\vec{E}$ is created perpendicular to the magnetic field $\vec{B}$ an $\vec{E} \times \vec{B}$

drift is introduced. The segmentation allows for an azimuthal rotation of the orientation of the applied electric dipole field. Changing the strength and orientation of the electric field allows the ion trajectory to be offset with respect to its original direction. The subsequent capture of the ion in a Penning trap leads to an initial magnetron motion. In this paper we discuss the basic features of such a Lorentz steerer, its design, operation, and performance.

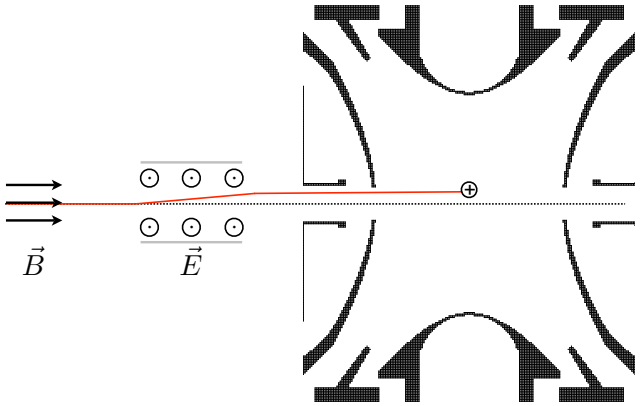

Fig. 1. Sketch illustrating a positively-charged ion passing through a region of perpendicular electric and magnetic fields, resulting in an off-axis capture in a Penning trap.

2 Charged particle motion in a region of perpendicular electric and magnetic fields

To begin we will consider the motion of a particle as it travels through a region of perpendicular electric and magnetic fields. Let $\vec{B} = \mathrm{B}\hat{z}$ and $\vec{E} = \mathrm{E}\hat{y}$. The equations of motion in the radial plane which must be solved are

$$\ddot{\vec{r}} = \frac{q}{m}(E\hat{y} + \dot{\vec{r}} \times B\hat{z}). \tag{1}$$

Consider a particle initially at the origin travelling in the $\vec{z}$ direction with no initial radial energy. The velocity in the radial plane and the radial displacement is then

$$\dot{r}(t) = \frac{\sqrt{2}E}{B}\sqrt{1-\cos(\omega_c t)} \tag{2}$$

$$r(t) = \frac{E}{B^2 q}\sqrt{2m^2[1-\cos(\omega_c t)] + [Bqt]^2 + 2mBqt\sin(\omega_c t)}, \tag{3}$$

where E is the strength of the electric field, q is the ionic charge, m is the mass, B is the strength of the magnetic field and ω_c = (q/m)B. For large values of t,

$$\lim_{t\to\infty} r(t) = \frac{E}{B}\cdot t = \bar{v}_{\text{drift}}\cdot t, \tag{4}$$

where $\bar{v}_{\text{drift}}$ is the average drift velocity of the ions. The displacement after travelling a distance L is proportional to $t = L/v_z \propto \sqrt{m}$.

For example, Fig. 2 plots the radial displacement as a function of time for an A = 40, singly-charged particle as it travels through a region of perpendicular, uniform electric, E = 28.6 V/m, and magnetic, B = 9.4 T, fields. This displacement is accompanied by a pickup of cyclotron motion which leads to the observed non-linearity. Fig. 3 plots the square of the radial velocity, which is proportional to the radial energy, of a particle as a function of ω_ct. From Eq. 2 it is shown that the radial velocity as a function of time scales as 1-cos(ω_ct). If we consider the particle to enter and exit the electric field suddenly, then upon exit it would have a radial velocity between 0 and $\sqrt{2}E/B$, depending upon the time of exit. Having left the electric-field region the ion performs a cyclotron motion with a radius that depends on the time of exit. For the example parameters used here the maximum radial velocity is V_r = 4300 m/s,

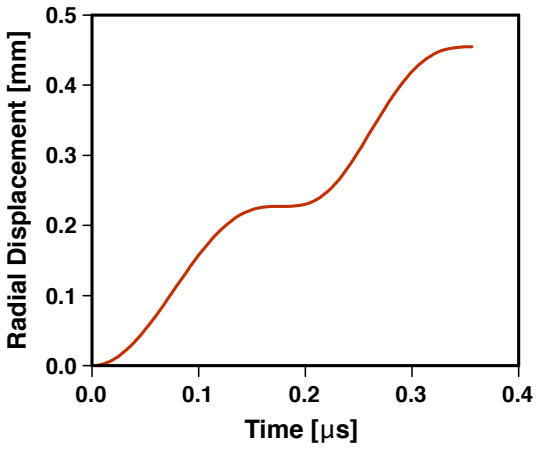

Fig. 2. Radial displacement as a function of time for a charged particle passing through a region of uniform, perpendicular electric and magnetic fields.

which corresponds to a radial energy $K_r = 5$ eV and a radius of the cyclotron motion of $\rho_{+,o} = 0.17$ mm.

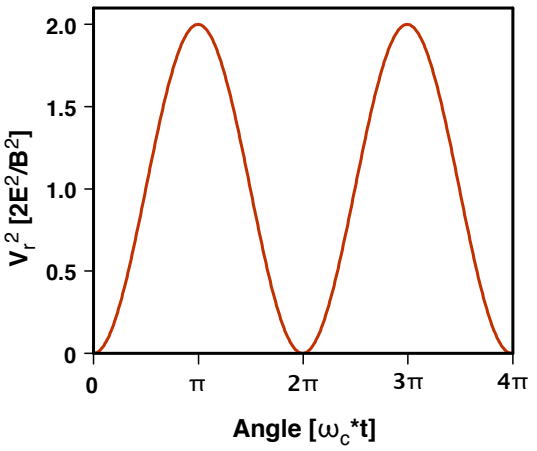

Fig. 3. Square of the radial velocity as a function of ω_ct of a charged particle after it has travelled through a region of uniform, perpendicular electric and magnetic fields.

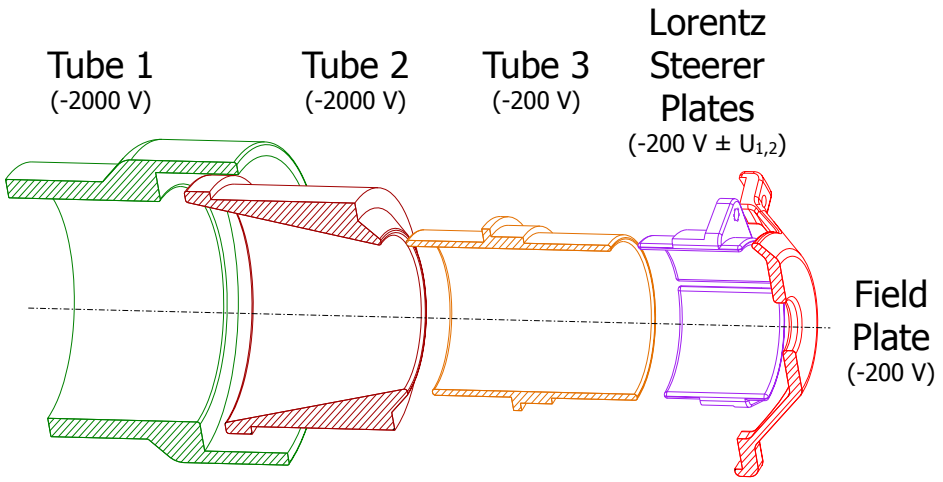

Fig. 4. Half-cut design drawing of the Lorentz steerer and nearby optics elements. The dashed line is the axis. Typical operating voltages are listed.

3 Lorentz steerer design

The design of the Lorentz steerer is remarkably simple, being four segments of a cylinder quartered in the radial plane. Fig. 4 shows a design drawing, half-cut, of a section of the injection optics of the LEBIT Penning trap mass spectrometer which contains the Lorentz steerer. The Lorentz steerer is located just previous to a field termination plate, and after a series of drift tubes. The steerer electrode system is 16.5 mm in length and 28 mm in diameter with 3 mm gaps between the four segments. Typical operating voltages are listed. These voltages were also used in SimIon simulations discussed later.

Fig. 5 shows a simple sketch of the electrode layout of the Lorentz steerer. Each pair of diametrically opposing electrodes can be used to generate an electric field with a dominant dipolar component. Changing the values of U_1 and U_2 such that $\sqrt{U_1^2 + U_2^2}$ remains constant results in a constant magnitude of the dipolar field, but changes its orientation in space. This imparts a constant radial displacement with an adjustable angle to ions passing through the

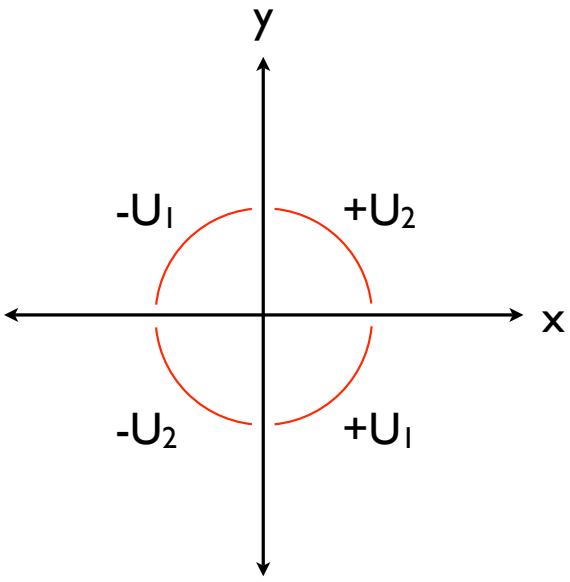

Fig. 5. Schematic layout of the Lorentz steerer's electrode configuration. Each pair of diametrically opposing electrodes can be used to create an electric dipole field. Both pairs can be used simultaneously to orient the dipole field in space.
steerer.

4 Lorentz steerer simulations

4.1 Calculation of ion beam deflection

The ion deflection in the Lorentz steerer has been calculated both analytically and numerically. While the magnetic field is assumed to be homogeneous, the electric field inside the steerer is required. One method is to use SimIon to numerically solve the Laplace equation in a geometry based on the design drawing shown in Fig. 4 and to trace the ions through the electric and magnetic fields. Another method to obtain the electric field is to analytically solve the

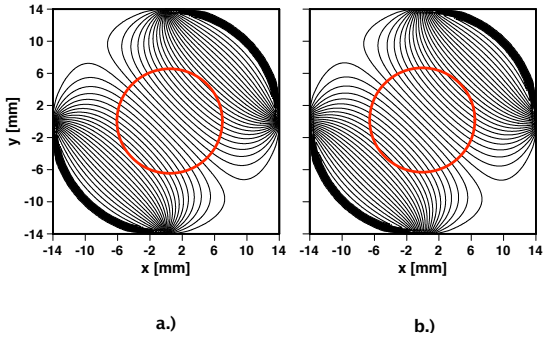

Fig. 6. Contour plots of the potential at the mid-plane of the Lorentz steerer given by a.) the analytical solution and b.) the SimIon calculation for $U_1 = 0$ V and $U_2 = 1$ V (see Fig. 5). Within a circle of radius of 6 mm the relative difference of the potentials obtained by both methods is less than 4×10^{-3}.

electric potential for an infinite quartered cylinder. This potential is given by

$$U(r,\phi) = \frac{U_1}{\pi}\left[\arctan\left(\frac{2Rr\sin(\phi)}{R^2-r^2}\right) - \arctan\left(\frac{2Rr\cos(\phi)}{R^2-r^2}\right)\right] + \tag{5}$$

$$\frac{U_2}{\pi}\left[\arctan\left(\frac{2Rr\sin(\phi)}{R^2-r^2}\right) + \arctan\left(\frac{2Rr\cos(\phi)}{R^2-r^2}\right)\right],$$

where R is the radius of the cylinder and U_1 and U_2 are the applied voltages. In order to account for the finite length of the Lorentz steerer the analytic potential given by this equation can be multiplied by a function f(z). From a comparison with the potential obtained with SimIon a function $f(z) = e^{(-z/\alpha)^4}$ with $\alpha = 1\times10^{-2}$ m was found to fit the potential along the axis well. Fig 6 plots the mid-plane potentials obtained from the SimIon calculation and the analytical solution for $U_2 = 1$ V and $U_1 = 0$ V. Within a 6 mm radius from the center of the steerer the potentials agree within $<4\times10^{-3}$.

A series of simulations was performed, using both the analytical and the Simion potentials, to study the properties of the realized Lorentz steerer. In

the case of the Simion simulations a geometry and potentials as shown in Fig. 4 was used. The initial ion distribution contained 500 ions and was centered on the axis of the Lorentz steerer. The width of the distribution in the radial direction was 0.1 mm. The ions started their flight in Tube 1, shown in Fig. 4, with an axial energy of 2 keV and no radial energy. After passing through the Lorentz steerer their radial positions were recorded at the location of the field plate.

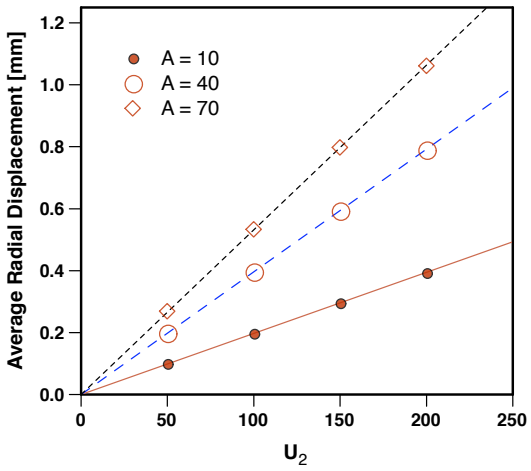

Fig. 7. Results of SimIon simulation showing mean radial displacement (data points) as a function of Lorentz steerer voltage (U_2) for three different masses. Lines are linear regressions.

Fig. 7 plots the mean radial displacement as a function of the potential applied to U_2 obtained from the SimIon simulations. As expected, the average radial displacement is proportional to U_2. The slopes of these lines represent a "steering strength" which depends on the mass and axial energy of the ion passing through the Lorentz steerer. Fig. 8 plots steering strength values obtained from the SimIon simulation (like those shown in Fig. 7). The solid line is the result of a calculation using the analytical solution for the potential of the quartered cylinder. There is good agreement between the SimIon simulations

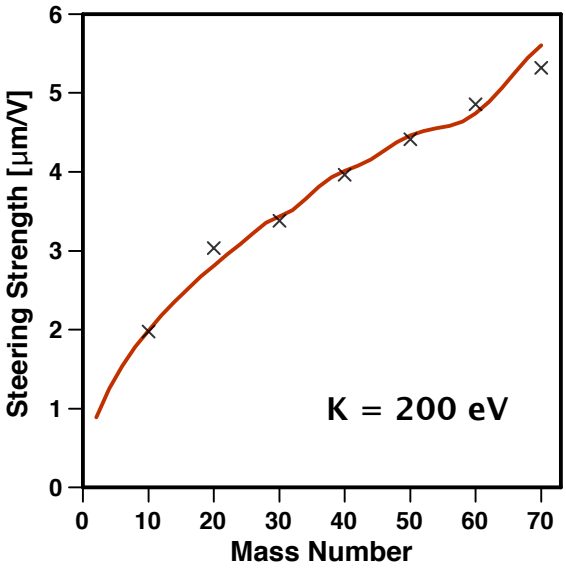

Fig. 8. Steering strength as a function of mass number of a singly-charged ion with K = 200 eV axial energy determined from SimIon simulations. The solid line is obtained using the analytical solution for the potential.
and the calculations.

4.2 How to achieve minimum cyclotron motion?

When injecting ions into a Penning trap it is important to introduce as little radial energy in the process as possible, as non-zero values of the initial cyclotron radius, $\rho_{+,o}$, can introduce asymmetries in the resonance line shape [11] and reduce the magnitude of the resonance signal. Fig. 9 plots the radial displacement as a function of time of an A = 70, singly-charged ion for two different of axial energies. The steering voltage was adjusted to result in the same final radial displacement. The curves were calculated using the analytical potential. The solid line is for an ion with K = 200 eV of axial energy and a steerer voltage $U_2 = 400$ V. The dashed line is for an ion with K = 50 eV of axial energy and a steerer voltage $U_2 = 200$ V. The K = 200 eV ion exits the

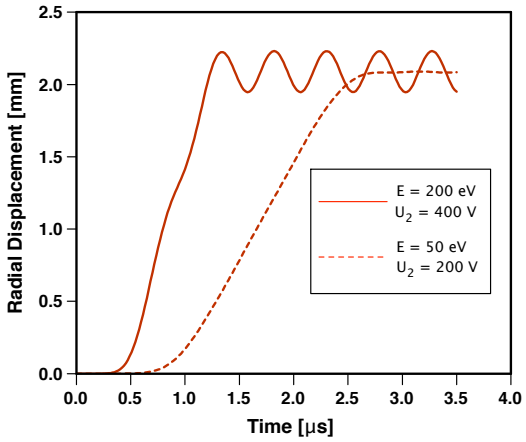

Fig. 9. Calculated radial displacement as a function of time for an A = 70, singly-charged ion as it travels through, and out of, the Lorentz steerer. The solid line is for a beam with K = 200 eV axial energy. The dashed line is for a beam with K = 50 eV axial energy. The steering voltages have been adjusted to result in the same final radial displacement.

electric field region after ≈ 1.25 μs. The oscillations are due to the induced cyclotron motion (see Sec. 2), in this case leading to an amplitude $\rho_{+,o} \approx 0.1$ mm. The slow ion exits the electric field region after ≈ 2.5 μs and achieves the same mean radial displacement as the fast ion, but with a cyclotron amplitude of $\rho_{+,o} \approx 2$ μm. Qualitatively this can be understood upon closer inspection of Eq. 2. Slower ions require more time to pass through the Lorentz steerer and therefore require a smaller electric field strength E to drive them to the same final radial displacement as a faster ion. For the system employed in the LEBIT Penning trap mass spectrometer an axial energy of less than 75 eV reduces the radial energy gain to sub-eV levels for the maximum applied steering voltages.

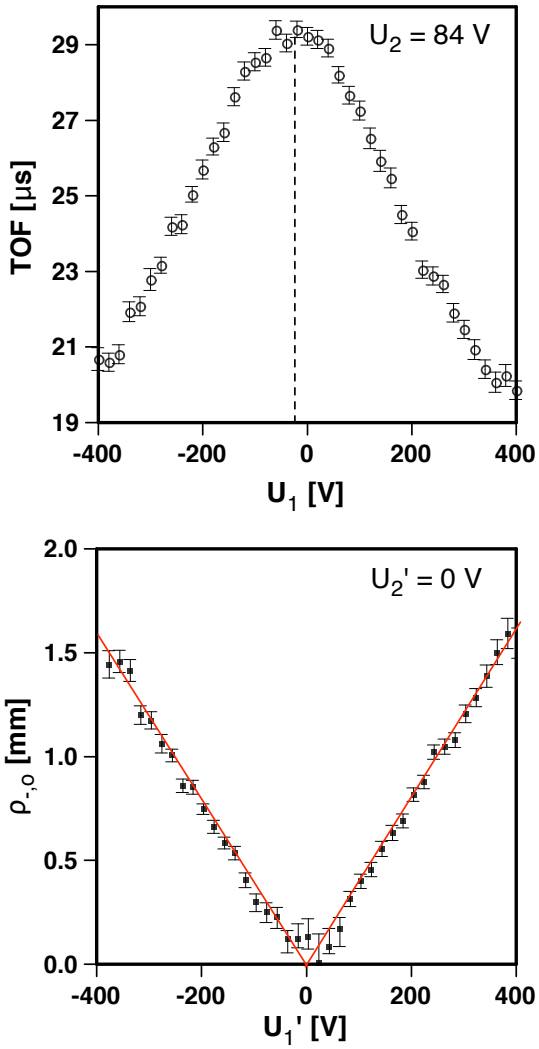

Fig. 10. Top: Time of flight of $^{39}K^{+}$ ions ejected from the trap after being subjected to a quadrupolar RF field with a frequency ν_c as a function of U_1 with U_2 = 84 V. Bottom: Initial magnetron amplitude, $\rho_{-,o}$, as calculated from the time-of-flight data shown above. $U_{1,2}$' are offset-corrected values of $U_{1,2}$ such that for $U_{1,2}$' = (0 V, 0V) the value of $\rho_{-,o}$ is minimized. Lines are to guide the eye and to illustrate the linearity of steering with applied voltage.

5 Lorentz Steerer Measurements

$^{39}K^{+}$ ions are created with a plasma ion source and delivered as short pulses using the LEBIT beam cooler and buncher [12]. After passing through the

Lorentz steerer the ions are captured in the Penning trap. If the ions enter the trap off axis then upon being trapped they perform an initial magnetron motion. Application of a π-pulse with frequency $\nu_{rf} \approx \nu_c$ can be used to completely convert the magnetron motion into cyclotron motions as discussed above. The accompanied increase in radial energy which can be detected via measurement of the time-of-flight of the ions [9] from the trap to a detector located outside of the magnetic field. By taking the radial energy gain and the known electric and magnetic fields traversed by the ion on its path to the detector, the value for the initial magnetron amplitude can be determined.

Fig. 10 (top) shows the time of flight of ejected $^{39}K^+$ ions as a function of voltage applied to the Lorentz steerer electrodes after capture in the trap and subsequent quadrupolar excitation for a time T_{rf} = 50 ms. U_2 was held at a constant 84 V for the following reasons. Due to imperfections in the injection of the ions into the magnetic field of the Penning trap spectrometer steering voltages of $U_1 = U_2 = 0$ do not necessarily correspond to injection on the trap axis, and an initial steering by the Lorentz steerer may be required. The values $U_{1,2}$ = (-24 V, 84 V) correspond to the maximum time of flight (and minimum initial magnetron amplitude). For ease of discussion we introduce offset-corrected steering voltages such that $U_{1,2}$' = (0 V, 0 V) corresponds to the maximum time of flight observed for $^{39}K^+$ ions.

Fig. 10 (bottom) shows the values of the initial magnetron amplitude calculated from the time-of-flight data in the above plot as a function of U_1'. The solid lines illustrate that the size of the magnetron radius $\rho_{-,o}$ of the captured ions is proportional to U_1', as expected from the simulation results shown in Fig. 7.

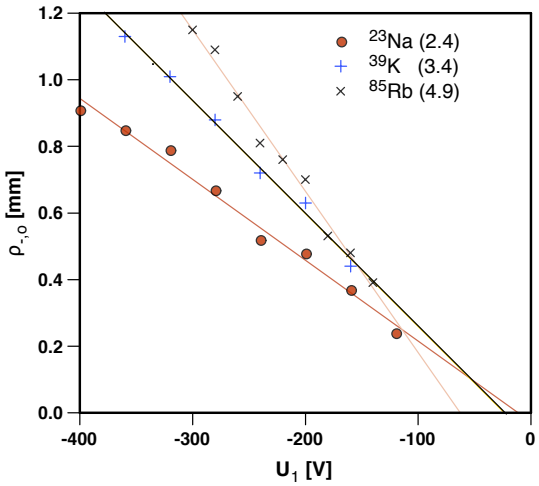

Fig. 11. Initial ρ_- as a function of U_1 for three different ion species. The numbers in parentheses are the steering strength values in μm/V.

Fig. 11 plots the results for the initial magnetron radius $\rho_{-,o}$ as a function of the true voltage U_1 obtained from measurements with three different ion species. The solid lines are linear fits to the data. The numbers in parentheses are the slopes of the lines which correspond to steering strength values (in μm/V). According to Eq. 4, the displacement respectively steering strength is proportional to $\sqrt{m}$ for ions with the same axial velocity. This is reflected in the experimental data and the measured steering strength values for ^{23}Na and ^{39}K also agree with the calculated values shown in Fig. 8.

The Lorentz steerer should allow for precision control not only of the amplitude of the magnetron motion, but of the initial phase, as well. In order to investigate how well this control works, an experiment was performed according to the following procedure. $^{39}K^+$ ions are placed off axis into the trap using the Lorentz steerer, resulting in an initial magnetron radius. Next a dipolar RF field, at frequency ν_-, which is phase-locked to the time of ion capture is applied. Depending on the phase of the RF field the excitation of the magnetron motion will result in a larger or smaller final magnetron radius. Using

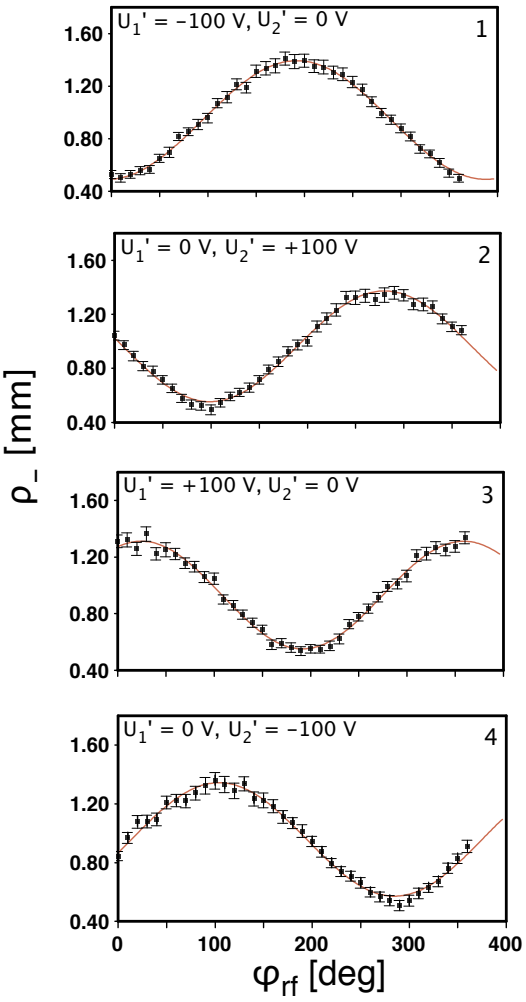

Fig. 12. Magnetron amplitude ρ_- as a function of ϕ_{rf} of $^{39}K^+$ ions subjected to a dipolar RF field at frequency ν_- for an excitation time of $T_{rf} = 50$ ms. The choice of steering voltages is such that, that the ions should be captured on a circle at angles 90° apart. Solid lines are sinusoidal fits to the data. The fit results are summarized in Table 1.

a π-pulse with $\nu_{rf} = \nu_c$ and the time-of-flight measurement allows the amplitude of the magnetron motion after the dipolar excitation to be determined. Fig. 12 presents the results of such a measurement. The magnetron amplitude ρ_- of $^{39}K^+$ ions is plotted as a function of the initial phase of the dipolar RF field for four different Lorentz steerer settings. Each setting corresponds to a

magnetron phase change of 90° from the previous setting and should provide the same steering strength. The data are fit with a sinusoidal function (solid line), $\rho_-(\phi) = \rho_{-,o} + \Delta\rho_- \cdot \sin(\phi_{rf} - \phi_{-,o})$, where $\rho_{-,o}$ is the initial magnetron amplitude introduced by the Lorentz steered, $\Delta\rho_-$ is the maximum amplitude change due to dipolar excitation, ϕ_{rf} is the initial phase of the RF, and $\phi_{-,o}$ is the initial magnetron phase. The fit results, given in Table 1, show that the initial magnetron amplitudes, $\rho_{-,o}$, due to the effect of the Lorentz steerer alone, agree to within a few percent. The phase change of 90° from one case to the next is confirmed to within ±2°. Both of these results together confirm that the ions were moved on a circle in the radial plane of the Penning trap and demonstrate the precision control of the initial ion placement in the trap available with the Lorentz steerer.

Table 1

Summary of the fit results of a fit of a sinusoidal function to the data presented in Fig. 12. $U_{1,2}$' are the offset-corrected voltages applied to the Lorentz steerer, $\rho_{-,o}$ is the initial magnetron amplitude given by the fit, $\phi_{-,o}$ is the initial magnetron phase given by the fit, and $\Delta\phi = |\phi^i_{-,o} - \phi^{i+1}_{-,o}|$ is the phase advance from one setting to the other.

	U_1' [V]	U_2' [V]	$\rho_{-,o}$ [mm]	$\phi_{-,o}$ [deg]	$\Delta\phi$ [deg]
1	-100	0	0.94(2)	102(1)	87(2.2)
2	0	+100	0.96(2)	189(2)	93(2.2)
3	+100	0	0.93(2)	282(1)	91(2.2)
4	0	-100	0.96(1)	13(2)	89(2.2)

6 Summary and Conclusions

A new technique for the precise manipulation of ion injection into a Penning trap has been developed and tested. It is used routinely in LEBIT's Penning trap mass spectrometer. Compared to the alternative method of magnetron preparation via dipolar excitation, it is less complicated and requires no additional preparation time. The Lorentz steerer offers complete control over the injection process and precise placement of an ion or a small ion cloud in the radial plane of a Penning trap. We expect that such a Lorentz steerer is a likely successor to dipolar excitation for magnetron preparation in future Penning trap systems. It is already foreseen in the TITAN [13] Penning trap mass spectrometer, presently under construction.

References

[1] G. Bollen, S. Becker, H.-J. Kluge, M. König, R. Moore, T. Otto, H. Raimbault-Hartmann, G. Savard, L. Schweikhard, H. Stolzenberg, Nucl. Instrum. Methods A 368 (1996) 675.

[2] G. Savard, R. C. Barber, D. Beeching, F. Buchinger, J. E. Crawford, S. Gulick, X. Feng, E. Hagberg, J. Hardy, V. T. Koslowsky, J. K. P. Lee, R. Moore, K. S. Sharma, M. Watson, Nucl. Phys. A 368 (1997) 353.

[3] V. S. Kolhinen, T. Eronen, J. Hakala, A. Jokinen, S. Kopecky, S. Rinta-Antila, J. Szerypo, J. Äystö, Nucl. Instrum and Methods in Phys. Res. B 204 (2003) 502.

[4] G. Sikler, D. Ackermann, G. Bollen, F. Attallah, D. Beck, J. Dilling, S. A. Eliseev, H. Geissel, D. Habs, S. Heinz, F. Herfurth, Nucl. Instr. and Meth. B

204 (2002) 482.

[5] R. Ringle, P. Schury, T. Sun, G. Bollen, D. Davies, J. Huikari, E. Kwan, D. Morrissey, A. Prinke, J. Savory, S. Schwarz, C. Sumithrarachchi, Int. J. Mass Spec. Ion. Proc. 251 (2-3) (2006) 300.

[6] I. Bergström, C. Carlberg, T. Fritioff, G. Douysset, J. Schonfelder, R. Schuch, Nucl. Instrum. Methods A 487 (2002) 618.

[7] G. Bollen, R. Moore, G. Savard, H. Stolzenberg, J. Appl. Phys. 68 (1990) 4355.

[8] M. König, G. Bollen, H.-J. Kluge, T. Otto, J. Szerypo, Int. J. Mass Spec. Ion. Proc. 142 (1995) 95.

[9] G. Gräff, H. Kalinowsky, J. Traut, Z. Phys. A297 (1980) 35.

[10] K. Blaum, G. Bollen, F. Herfurth, A. Kellerbauer, H.-J. Kluge, M. Kuckein, S. Heinz, P. Schmidt, L. Schweikhard, J. Phys. B: At. Mol. Opt. Phys. 36 (2003) 921.

[11] R. Ringle, G. Bollen, P. Schury, S. Schwarz, T. Sun, Int. J. Mass Spec. in publication.

[12] T. Sun, S. Schwarz, G. Bollen, D. Lawton, R. Ringle, P. Schury, Eur. Phys. J. A 25(S1) (2005) 61.

[13] J. Dilling, R. Baartman, P. Bricault, M. Brodeur, L. Blomeley, F. Buchinger, J. Crawford, J. Crespo López-Urrutia, P. Delheij, M. Froese, G. Gwinner, Z. Ke, J. K. P. Lee, R. Moore, V. Ryjkov, G. Sikler, M. Smith, J. Ullrich, J. Vaz, Int. J. Mass Spec. 251 (2006) 198.